



CHORUS

This is the accepted manuscript made available via CHORUS. The article has been published as:

High-Resolution ac Measurements of the Hall Effect in Organic Field-Effect Transistors

Y. Chen, H. T. Yi, and V. Podzorov

Phys. Rev. Applied **5**, 034008 — Published 17 March 2016

DOI: [10.1103/PhysRevApplied.5.034008](https://doi.org/10.1103/PhysRevApplied.5.034008)

High-resolution *ac* measurements of the Hall effect in organic field-effect transistors.

Y. Chen^{1,†}, H. T. Yi¹ and V. Podzorov^{1,2,*}

¹ Department of Physics, Rutgers University, Piscataway, New Jersey 08854, USA.

² Institute for Advanced Materials and Devices for Nanotechnology (IAMDN), Rutgers University, Piscataway, New Jersey 08854, USA.

* Corresponding author: podzorov@physics.rutgers.edu

We describe a high resolving power technique for Hall effect measurements, efficient in determining Hall mobility and carrier density in organic field-effect transistors and other low-mobility systems. We utilize a small low-frequency *ac* magnetic field ($B_{\text{rms}} < 0.25$ T) and a phase sensitive (lock-in) detection of Hall voltage, with the necessary corrections for Faraday induction. This method significantly enhances signal-to-noise ratio and eliminates the necessity of using high magnetic fields in Hall effect studies. With the help of this method, we were able to obtain Hall mobility and carrier density in organic transistors with mobility as low as $\mu \sim 0.3 \text{ cm}^2\text{V}^{-1}\text{s}^{-1}$ by using a compact desktop apparatus and low magnetic fields. We have found a good agreement between Hall effect and electric field-effect measurements, indicating that contrary to the common belief, certain organic semiconductors with mobilities below $1 \text{ cm}^2\text{V}^{-1}\text{s}^{-1}$ can still exhibit a fully developed, band-semiconductor like Hall effect, with the Hall mobility and carrier density matching those obtained in longitudinal transistor measurements. This suggests that even when $\mu < 1 \text{ cm}^2\text{V}^{-1}\text{s}^{-1}$, charges in organic semiconductors can still behave as delocalized **coherent** carriers. This technique paves way to ubiquitous Hall effect studies in a wide range of low-mobility materials and devices, where it is typically very difficult to resolve Hall effect even in very high *dc* magnetic fields.

[†] Current address: Dept. of Physics, South University of Science and Technology of China, Shenzhen, Guangdong, China.

I. INTRODUCTION

Charge carrier transport in organic semiconductors frequently occurs at the borderline between a band-like coherent motion through extended states and an incoherent hopping via localized states. Intrinsic factors competing for determining the dominant transport mechanism include intermolecular π - π interactions governed by the equilibrium crystal packing (the transfer integrals) [1], carrier self-localization due to the local electron-phonon coupling in the form of polarons [2, 3, 4], as well as non-local electron-phonon coupling and off-diagonal thermal disorder [5, 6]. In molecular crystals with sufficiently strong intermolecular interactions, bands of delocalized states can form, leading to a band-like transport, provided that thermal disorder is not too strong (see, e.g., [7] and refs. therein). However, because of weak van der Waals interactions, such bands are typically narrow (a few hundred meV), and the carrier mobility, μ , is intrinsically low ($\mu \sim 0.1 - 20 \text{ cm}^2\text{V}^{-1}\text{s}^{-1}$) [1,7] in comparison with inorganic semiconductors, where μ is usually in the range 100 - 2000 $\text{cm}^2\text{V}^{-1}\text{s}^{-1}$ [8]. Thermal disorder can play a dual role: while promoting carrier hopping among molecules in the activated hopping regime, it tends to destroy the extended bands that might exist otherwise and lead to carrier localization and scattering, thus creating localized states below the mobility edge (the tail states) [5,6,9,10]. Such localized tail states do contribute to charge transport by providing a hopping pathway for carriers and participating in multiple trap and release processes [7]. It is believed that a crossover between the hopping and band-like transport regimes occurs in organic field-effect transistors (OFET) when the charge carrier mobility is around unity, $\mu \sim 1 \text{ cm}^2\text{V}^{-1}\text{s}^{-1}$. Besides these intrinsic factors, static disorder originated from chemical impurities and structural defects also plays a significant role in real-world materials, usually leading to additional trap states in the tail that immobilize charge carriers at various time scales [9, 11, 12].

Hall effect represents a powerful tool for the studies of the intrinsic charge transport properties of organic semiconductors, because the Lorenz force acting on drifting charge carriers in Hall measurements only acts on delocalized (that is, band-like) charge carriers that have a non-zero microscopic drift velocity, while localized (hopping) carriers are not expected to contribute to Hall voltage by means of a classical Lorenz force (for a review on Hall effect and transport studies in single-crystal OFETs see, e.g., [7] and refs. therein; **for individual Hall effect studies in various OFETs see [13, 14, 15, 16, 17]**). It would only be fair however to mention that a transverse magnetic field effect in purely hopping transport regime, originating from quantum

interference effects on the hopping probabilities in closed-loop trajectories, has been theoretically predicted [18], but thus far eluded experimental observations [19]. Thus, a classical (band-semiconductor like) Hall effect observed in an OFET is expected to probe delocalized charge carriers in extended band states and can therefore: (a) reveal if such band states exist in the system, and (b) give information about the concentration and the intrinsic mobility of charges in these states. Despite the importance of Hall effect, however, such studies are not widely pursued in organic semiconductors, because it is typically very difficult to resolve Hall voltage in these highly resistive low- μ materials even in high magnetic fields. For example, a Hall voltage presented in an OFET under typical experimental conditions is $V_{\text{Hall}} = W \cdot E_{\text{SD}} \cdot B \cdot \mu$, where $W \sim 0.1 - 1$ mm is the channel width in a typical Hall bar geometry, $E_{\text{SD}} = 10 - 100 \text{ V}\cdot\text{cm}^{-1}$ is the longitudinal source-drain electric field, B is the magnetic field (typically up to 12 T), and $\mu \sim 1 \text{ cm}^2\text{V}^{-1}\text{s}^{-1}$ is the mobility in systems at the borderline between hopping and band-like transport, thus giving a typical $V_{\text{Hall}} \sim 0.1 - 10$ mV. Electric noise due to carrier hopping and shallow traps can be rather significant and can easily mask the small Hall voltage. Therefore, it is usually very difficult to extract the small Hall signal from a noisy background in OFETs, even if one uses a superconducting magnet and a very high magnetic field of up to 12 T [13,14,15,16,17]. Below, we describe an *ac* Hall effect measurement technique that we have developed for OFETs and other low- μ systems. We show that in comparison with the conventional *dc* Hall measurements, this method delivers a much more superior signal/noise ratio, especially important for Hall effect studies in low-mobility materials and devices. It is also technically important that high magnetic fields are not necessary in this method. The paper is organized as follows. Section II provides technical details of device fabrication and measurements. Section III describes the charge transport properties of single-crystal OFETs used in this study, as well as provides a description of our *ac* Hall measurement setup. Section IV describes the basic concept of a phase sensitive detection of Hall voltage induced by an *ac* magnetic field and gives the details of our Faraday induction corrected *ac* Hall effect measurements. In section V, we discuss the results obtained for two types of OFETs and compare the carrier densities and mobilities measured using the longitudinal OFET transport and the *ac* Hall effect. Section VI gives the conclusions.

II. METHODS

Rubrene and tetracene single crystals were grown using a physical vapor transport method in a stream of ultra-high purity He gas at sublimation temperature of 320 and 280 °C, respectively (for details see, e.g., [7]). For OFET fabrication, electrical contacts were painted on the (*a,b*) facets of the crystals with an aqueous solution of colloidal graphite (Ted Pella) and contacted with 25 mm-thick gold wires. In tetracene OFETs, we used a very thin under-layer of Cytop (< 30 nm) topped with a much thicker layer of parylene-*N* (1.35 μm) as a gate insulator (capacitance, $C_i = 1.7 \text{ nF}\cdot\text{cm}^{-2}$). Cytop was deposited by spin coating a commercially available Cytop precursor solution at 3000 rpm for 300 s on a flat crystal attached to a solid glass substrate with a thermal wax, followed by a gentle overnight annealing at 60 °C in vacuum, which resulted in uniform thin films with a thickness of less than 30 nm. Using Cytop under-layer gave better signal-to-noise ratio in Hall voltage measurements in tetracene OFETs. In rubrene OFETs, only parylene-*N* gate dielectric (with a typical thickness 1 - 1.1 μm) was used ($C_i = 2.1 - 2.3 \text{ nF}\cdot\text{cm}^{-2}$). Gate electrodes were prepared by thermally evaporating silver (35 nm-thick) through a shadow mask on top of the parylene coated crystals. Typical aspect ratios of the channel dimensions in our OFETs were: $L/W = 1 - 3$, $D/W = 0.4 - 0.7$, where L is the channel length, W is the channel width, and D is the longitudinal distance between the 4-probe voltage probes. All measurements reported in this study were performed at room temperature in air. Keithley Source-Meters K-2400 and Electrometers K-6512 were used for FET measurements. In *ac* Hall measurements, we used DL1201 voltage preamplifier (DL Instruments) and Stanford Research SR-830 lock-in amplifier for Hall voltage measurements, Keithley current source K6221 for I_{SD} excitation, and Electrometer K6514 for 4-probe voltage measurements. *ac* magnetic field of a frequency 0.5 - 3 Hz with a root-mean-square magnitude of $B_{\text{rms}} = 0.23 \text{ T}$ has been generated by rotating an assembly of strong permanent Nd magnets fixed on an Al frame. The magnet assembly is driven by a *dc* electro-motor (Dayton 3XE22D), which is in turn controlled by a Hewlett Packard *dc* power supply HP 6642A. Rotation speed can be adjusted by varying the output voltage of the power supply. $B(t)$ near the sample is measured in real time by a Bell-5180 Gauss meter, which also generates an output voltage proportional to $B(t)$. We use this voltage as a reference signal for the lock-in. Data acquisition was carried out by interfacing the instruments with a computer through a National Instruments GPIB card controlled by a LabVIEW program.

III. SINGLE-CRYSTAL OFETS AND AC HALL EFFECT SETUP

Rubrene (C₄₂H₂₈) and tetracene (C₁₈H₁₂) OFETs used in this study are the top-contact/top-gate devices fabricated on macroscopic vapor-grown single crystals of rubrene and tetracene using graphite paint contacts, low- ϵ polymers as gate insulators and evaporated silver gates. For gate dielectrics, we used either 1.1 - 1.35 μm -thick parylene- N films or a combination of extremely thin (< 30 nm) Cytop and a thick (~ 1.35 μm) parylene- N (for fabrication details see sec. II Methods). For characterization of these OFETs, transconductance characteristics (the channel source-drain current, I_{SD} , as a function of the gate voltage, V_G , at a given source-drain voltage, V_{SD}) were recorded in the linear and saturation regimes to extract the carrier mobility, μ , according to the standard (2-probe) FET equations (see, e.g., [7]):

$$I_{SD}^{lin} = \frac{W}{L} \mu_{lin} C_i V_{SD} (V_G - V_T) \quad (|V_G| \gg |V_{SD}|), \quad I_{SD}^{sat} = \frac{W}{2L} \mu_{sat} C_i (V_G - V_T)^2 \quad (|V_G| < |V_{SD}|), \quad (1)$$

where L and W are the channel's length and width, respectively, C_i is the gate-channel capacitance per unit area ($C_i = 1.7$ nF·cm⁻² in our tetracene OFETs, and, depending on the exact thickness of the dielectric, 2.1 - 2.3 nF·cm⁻² in our rubrene OFETs), and V_T is a threshold voltage, which is typically small in single-crystal OFETs. Thus, the carrier mobility in the linear and saturation regimes, μ_{lin} and μ_{sat} , as well as the total carrier density (electrostatically induced above the threshold), n_{FET} , can be found using the following expressions:

$$\mu_{lin} = \frac{L}{W} \frac{1}{C_i} \frac{1}{V_{SD}} \frac{\partial I_{SD}}{\partial V_G}, \quad \mu_{sat} = \frac{2L}{W} \frac{1}{C_i} \left(\frac{\partial \sqrt{|I_{SD}|}}{\partial V_G} \right)^2, \quad en_{FET} = C_i (V_G - V_T) \quad (2)$$

Figures 1 and 2 show the electric characteristics of the rubrene and tetracene OFETs similar to those used in the present study. Both systems exhibit a standard text-book FET behavior, well described by the above equations, with an extended linear regime in $I_{SD}(V_G)$, in which the mobility is nearly independent of the carrier density and the longitudinal electric field (that is, μ is independent of V_G and V_{SD} , respectively). In the saturation regime, this corresponds to a linear "square-root" transfer curve, $|I_{SD}|^{1/2}(V_G)$. The existence of such an extended linear regime is crucial for the correct and reliable extraction of the longitudinal drift field-effect mobility in OFETs. In both types of devices, a good match between the linear and saturation mobilities is observed, $\mu_{sat} \approx \mu_{lin}$. Typical mobility at the rubrene/parylene- N interface is around 5 - 6 cm²V

s^{-1} , while the typical mobility at the tetracene/Cytop interface is in the range $0.3 - 0.8 \text{ cm}^2\text{V}^{-1}\text{s}^{-1}$. These values are consistent with the dielectric permittivities of parylene- N ($\epsilon = 2.6$) and Cytop ($\epsilon = 2$) and with the mobilities obtained in similar single-crystal OFETs in the prior studies [7,20,21,22,23]. It is worth noting that mobilities obtained in our devices by a gated 2-probe technique are similar to the 4-probe mobilities, indicating that the contact resistance is relatively small.

In our *ac* Hall measurements, an *ac* magnetic field is generated by rotating strong permanent neodymium (Nd) magnets, rigidly assembled on an aluminum frame. The sample is wired inside of a light-proof thin aluminum box, which is placed in the gap between the rotating magnets, so that the magnetic field is perpendicular to the OFET's accumulation channel (a sketch and a photo of the setup are shown in Fig. 3; a video of the setup in operation is available at [24]). The rotation is driven by a *dc* electric motor. A gauss probe placed near the sample is used to measure the magnetic field, $B(t)$, and its frequency ω in real time. It generates a small output voltage proportional to $B(t)$, which is supplied back to the lock-in amplifier as a reference. This method of generating *ac* B field is more convenient than using electromagnets, in which case specially designed coils and powerful current sources are necessary to achieve magnetic fields greater than 0.2 T. Even if the frequency of magnet rotation slightly fluctuates over time, the lock-in amplifier tracks the actual frequency, which allows the powerful noise discrimination provided by the phase sensitive detection to be fully utilized without the use of high-precision step motors. In our system, fluctuations of ω are typically slow and are within 2% of its average value. In the case when the generated *ac* magnetic field $B(t)$ is periodic but not exactly harmonic (that is, does not exactly follow a sine or cosine), the magnetic field amplitude that defines the measured *ac* Hall voltage is given by the first Fourier harmonic of $B(t)$ function (at the frequency ω), which can be determined either analytically by taking a Fourier transform of the measured $B(t)$ or experimentally by performing spectrum analysis using an oscilloscope or a spectrum analyzer. In our setup, this harmonic corresponds to the root-mean-square (*rms*) magnetic field $B = 0.23 \text{ T}$. The *ac* Hall voltage across the channel is measured by a lock-in amplifier tuned to the frequency of the B field tracked by the Gauss meter. The longitudinal *dc* source-drain voltage, 4-probe voltage and *dc* source-drain current are applied/measured by Keithley source-meters and electrometers.

IV. AC HALL EFFECT MEASUREMENTS IN OFETS

Phase sensitive (lock-in) detection technique is widely used to extract small signals from a noisy background, whose fluctuations are often orders of magnitude larger than the signal of interest. In electric measurements, the most common practice is to drive an *ac* excitation current, I , through the sample and measure the desired voltage that is phase-locked to the excitation. However, this specific implementation of phase sensitive detection does not solve the problem of poor signal-to-noise ratio in conventional Hall effect measurements. Indeed, with an *ac* current excitation, the true Hall voltage across the channel, $V_{\text{Hall}} \propto I \cdot B$, and the parasitic offset voltage due to unavoidable longitudinal misalignment (or asymmetry) of Hall probes, $V_{\text{offset}} \propto I \cdot R_{\text{offset}}(B)$, where $R_{\text{offset}}(B)$ is some effective sample resistance between the misaligned Hall leads, are both modulated at the frequency of the excitation. Therefore, a phase sensitive detection in this case would not be able to discriminate the true Hall voltage (the signal) from the fluctuating offset (the noisy background). The correct method would thus use an *ac* magnetic field, $B = B_0 \cdot \cos(\omega t)$, applied perpendicular to the channel, while driving a *dc* longitudinal excitation current through the sample (Fig. 3). In that case, V_{Hall} is modulated at the frequency of the B field, whereas V_{offset} shows either no modulation (if there is no magneto-resistance) or changes at higher harmonics (2ω , 4ω , 6ω , etc), because magneto-resistance of most materials is an even function of B and thus does not lead to a signal at the first harmonic. Phase sensitive detection can then be used to selectively measure the true Hall voltage.

In general, the total voltage across the Hall probes, V_{H} , is composed not only of the true *ac* Hall voltage, V_{Hall} , but also an *ac* Faraday induction electromotive force, V_{F} , because the electric circuit connected to the Hall probes forms a closed loop, through which an *ac* magnetic field passes. The magnitude of the Faraday induction depends on both the frequency of the magnetic field and the effective area, S , of the loop: $V_{\text{F}} \propto -S \cdot dB/dt = S \cdot B_0 \omega \cdot \sin(\omega t)$. This parasitic signal can be minimized by carefully wiring the sample in such a way that the area of the loop S is as small as possible and by performing measurements at low frequency. In addition, most organic samples have rather high resistivity, which gives another reason for working at low frequencies: parasitic capacitance distributed over the measurement circuit may shunt sample impedance at high frequencies. Usually, $f = \omega/2\pi \sim 0.5 - 2.5$ Hz should be used for most OFETs. Nevertheless, even when working at a low frequency with carefully minimized wiring loop, the

Faraday induction may still be comparable to or even greater than the true Hall signal, especially in low-mobility samples with $\mu < 1 \text{ cm}^2\text{V}^{-1}\text{s}^{-1}$. Fortunately, Faraday induction signal is rather stable, since the fluctuations in ω are typically less than 2%, and the loop area enclosed by the wires is constant for a given measurement. Therefore, V_F can be measured as a stable background at zero excitation current (that is, at $V_{SD} = I_{SD} = 0$, yet with the gate voltage applied, which in p -type OFETs corresponds to $V_G < 0$). At these conditions, the true Hall voltage is zero, $V_{\text{Hall}} = 0$. V_F can then be subtracted from the total signal, V_H , measured at a finite excitation ($V_{SD}, I_{SD} > 0$) and at the same $V_G < 0$. In addition, we note that according to its definition, the Faraday induction is phase shifted with respect to B and the true V_{Hall} by $\pi/2$, which provides an additional way of discriminating it from the true Hall voltage (Fig. 4a).

Phase sensitive detection measures both the *rms* magnitude and the phase angle of the total voltage presented across the Hall voltage leads, V_H , with respect to the reference signal proportional to $B(t)$. Alternatively, it measures V_H 's x and y components, V_H^x and V_H^y (note that x and y superscripts here do not refer to the real-space coordinates, but rather correspond to the two signals detected on the lock-in's X and Y channels, with the x -channel being in-phase with the reference signal and y -channel being phase shifted by $\pi/2$). In our setup, in the ideal situation of a negligible parasitic capacitance, the true Hall voltage has a phase angle zero (only x component), and the Faraday induction has a phase angle 90° (only y component). This is because Hall voltage is proportional to B , whereas Faraday induction is proportional to dB/dt . In reality, however, phase angles of both the true Hall voltage and the Faraday induction show some small deviation from the above ideal values, which is schematically depicted at Fig. 4a, and thus, $V_H^x = V_{\text{Hall}}^x + V_F^x$, and $V_H^y = V_{\text{Hall}}^y + V_F^y$. Therefore, the proper way of extracting *rms* value of the pure Hall voltage, V_{Hall} , is to perform a vector subtraction of the background signal measured at $I_{SD} = 0$ (the Faraday induction only, V_F) from the total signal measured at $I_{SD} > 0$ ($V_H = V_{\text{Hall}} + V_F$):

$$|V_{\text{Hall}}| \equiv \sqrt{(V_{\text{Hall}}^x)^2 + (V_{\text{Hall}}^y)^2} = \sqrt{(V_I^x - V_0^x)^2 + (V_I^y - V_0^y)^2}, \quad (3)$$

where V_I and V_0 are the total voltages measured between the Hall leads at $I_{SD} \neq 0$ and $I_{SD} = 0$, respectively. Thus, we perform cycles of measurements, each composed of a zero-current stage followed by a finite-current stage, with several cycles usually taken to average the obtained true V_{Hall} signal (Fig. 4b). A dedicated LabVIEW program records the x and y lock-in signals in the

off and *on* stages, performs a vector subtraction according to the Eq. 3 and extracts the correct Hall carrier density and mobility according to the formulas:

$$n_{\text{Hall}} = \frac{I_{\text{SD}} \cdot B}{eV_{\text{Hall}}} = \frac{\sigma_{4p} \cdot B}{e} \cdot \frac{W}{D} \cdot \frac{V_{4p}}{V_{\text{Hall}}}, \quad \mu_{\text{Hall}} \equiv \frac{\sigma_{4p}}{en_{\text{Hall}}} = \frac{1}{B} \cdot \frac{D}{W} \cdot \frac{V_{\text{Hall}}}{V_{4p}}, \quad (4)$$

where the *ac* variables B and V_{Hall} are taken in their *rms* form (that is, here, $B = 0.23$ T and V_{Hall} defined by Eq. 3), σ_{4p} is the 4-probe channel conductivity per square, D is the distance between the voltage probes in the 4-probe configuration, V_{4p} is the 4-probe voltage (other parameters are defined above).

Figure 4b shows an example of *ac* Hall voltage recorded in two stages, $I_{\text{SD}} = 0$ and 10 nA, in a pristine single-crystal rubrene OFET with parylene gate insulator, performed at $V_{\text{G}} = -20$ V, $V_{\text{SD}} = 0.1$ V and $B_{\text{rms}} = 0.23$ T ($f = 0.57$ Hz). Here, we use crystalline rubrene as our test material, because since their discovery in 2003 [21,22], rubrene OFETs represent benchmark high-performance organic transistors, well characterized in various device configurations [7,13,14,16,25]. In this measurement, an extremely small Hall voltage of 6.35 μV is easily resolved. We note that the observed Hall voltage is more than three orders of magnitude smaller than V_{Hall} estimated above for conventional Hall measurements in a high *dc* magnetic field of 10 T, which makes sense, because the other parameters in our experiment (B and I_{SD}) are extremely small. Yet, it results in the correct Hall carrier density and mobility, comparable to those obtained in rubrene OFETs by the conventional Hall effect technique [13,14]. The important distinction here is that the signal-to-noise ratio in our *ac* Hall method is much superior to that in the conventional *dc* Hall measurements. The mobility and carrier density extracted from the data in Fig. 4b are $\mu_{\text{Hall}} = 5.8 \pm 0.05 \text{ cm}^2\text{V}^{-1}\text{s}^{-1}$ and $n_{\text{Hall}} = (2.26 \pm 0.02) \times 10^{11} \text{ cm}^{-2}$, which agree well with the results obtained in longitudinal 4-probe OFET measurements of the same device (Fig. 6, for example). This demonstration shows the remarkable resolving power of *ac* Hall effect technique described here.

Although the above procedure allows to largely get rid of the Faraday induction artifacts in *ac* Hall measurements, we find that an additional measurement, a frequency dependence, is necessary in certain cases of low-mobility OFETs or OFETs with a significant contact resistance. Indeed, the vector subtraction procedure described earlier assumes that the Faraday induction signal is the same (phase- and amplitude-wise) in the *on* and *off* stages of the measurement. This should indeed be the case in “ideal” or “well-behaved” FETs, as long as the same gate voltage is

applied during both stages. Such a situation is realized, for instance, in rubrene single-crystal OFETs, where an efficient carrier injection from contacts occurs even at zero source-drain bias ($V_{SD} = I_{SD} = 0$), and an accumulation channel is formed, as long as $V_G < 0$ is applied [7,22]. In such a case, the portion of the accumulation channel between the Hall voltage probes that “connects” them together, thus forming a closed loop, has the same density of charge carriers, resistivity, capacitance and inductance at both *on* and *off* stages. However, this may not be the case in OFETs with large Schottky contact barriers, where a significant source-drain voltage must be applied, in addition to V_G , to inject carriers and form an accumulation channel. Besides, in the systems dominated by shallow traps or tail states, carrier mobility may steeply depend on the longitudinal electric field, which can make the channel conductivity to be different at the *on* and *off* stages [26]. In such cases, we find that the apparent *ac* Hall voltage exhibits a linear dependence on frequency, signaling that not all of the Faraday induction has been removed by the data analysis discussed earlier. The linear dependence however allows us to unambiguously determine the true Hall mobility by extrapolating $\mu_{\text{Hall}}^{\text{ac}}(f)$ dependence to $f = 0$ (zero-frequency limit), at which the Faraday induction contribution is zero. This zero-frequency offset corresponds to the true Hall mobility, μ_0 . Therefore, the correct *ac* Hall measurements in OFETs should include a frequency dependent measurement to find a zero-frequency offset.

Examples of such f -dependent measurements are shown in Fig. 5 for pristine rubrene and tetracene single-crystal OFETs. The rubrene OFET does not exhibit any frequency dependence, with the true Hall mobility $\mu_0 = 5.1 \text{ cm}^2\text{V}^{-1}\text{s}^{-1}$ (Fig. 5a), while the tetracene OFET does show a frequency dependence with a finite zero-frequency offset corresponding to the true Hall mobility of $\mu_0 = 0.3 \text{ cm}^2\text{V}^{-1}\text{s}^{-1}$ (Fig. 5b). It is worth noting that in tetracene OFETs, measurements at an increasing V_{SD} result in a weaker frequency dependence, which is consistent with the notion of a suppressed contact resistance at a higher source-drain voltage in OFETs [22]. We note that transistors that do not have delocalized charge carriers (such as in a purely hopping regime) are not expected to exhibit a classical Hall effect. Although a non-zero (apparent) *ac* Hall voltage at finite frequencies is expected in such devices due to the small residual Faraday induction, taking a zero-frequency limit should result in $V_{\text{Hall}} = 0$ and $\mu_0 = 0$ (a straight line passing through the origin). Thus, performing the frequency dependence check in *ac* Hall effect studies is important. In all further discussions of the *ac* Hall measurements below, we use either zero-frequency offsets or values obtained at the lowest frequency of 0.5 Hz, at which the error is negligible.

V. COMPARISON OF FET AND AC HALL EFFECT MEASUREMENTS

Figures 6 and 7 present a comparison between the *ac* Hall effect and FET measurements of rubrene and tetracene single-crystal OFETs. As described in sec. III, both rubrene and tetracene OFETs studied here exhibit a text-book FET behavior with an extended linear regime in $I_{SD}(V_G)$ characteristics, signifying a mobility nearly independent of the carrier density (seen as the plateaus in Figs. 6a and 7a). We emphasize that such a linear regime is crucial for an unambiguous extraction of the longitudinal field-effect drift mobility (for other criteria of applicability of the standard FET equations 1 and 2 see, e.g., [7]). The drift mobility extracted from the saturation regime measurements matched well that obtained in the linear regime, $\mu_{\text{sat}} \approx \mu_{\text{lin}}$. For details of these transistor measurements see sec. III.

ac Hall effect measurements in these representative single-crystal OFETs yield Hall mobilities and carrier densities matching those obtained from the conventional longitudinal FET measurements (Figs. 6 and 7), thus suggesting that Hall effect in these OFETs is fully developed. It is worth noting that an under-developed Hall effect, characterized with $\mu_{\text{Hall}} < \mu_{\text{FET}}$ and $n_{\text{Hall}} \equiv (I_{\text{SD}}B) \cdot (eV_{\text{Hall}})^{-1} > n_{\text{FET}} \equiv e^{-1} \cdot C_i(V_G - V_T)$, has been reported for several organic semiconductors, including pentacene [27]. These observations have prompted an empirical conclusion that an under-developed Hall effect typically occurs in systems where off-diagonal thermal disorder is sufficiently strong to lead to a *partial* carrier coherence. The carrier coherence can be parametrized by a coherence factor, α , defined as the ratio of the total carrier density above the threshold, n_{FET} , to the carrier density extracted from the Hall effect measurements, n_{Hall} . In systems with under-developed Hall effect, the carrier coherence factor is thus $\alpha < 1$, while in systems with a fully developed Hall effect, $\alpha \approx 1$ [7,27,28]. The microscopic details of partial carrier coherence require further investigation, although it is believed that organic semiconductors at the borderline between band and hopping transport, characterized with a low carrier mobility of $\mu \sim 1 \text{ cm}^2\text{V}^{-1}\text{s}^{-1}$, would be more prone to exhibiting an under-developed Hall effect ($\alpha < 1$), compared to the systems with a high charge carrier mobility of $\mu \sim 5 - 20 \text{ cm}^2\text{V}^{-1}\text{s}^{-1}$. Indeed, in several cases of high-mobility organic semiconductors, Hall effect has been reported to be fully developed, $\mu_{\text{Hall}} \approx \mu_{\text{FET}}$ and $n_{\text{Hall}} \approx n_{\text{FET}}$ ($\alpha \approx 1$) (see, e.g., [7,28]). The surprising observation in this work is that a system with a very low carrier mobility $\sim 0.3 \text{ cm}^2\text{V}^{-1}\text{s}^{-1}$

$\text{cm}^2\text{V}^{-1}\text{s}^{-1}$ (tetracene OFETs) not only shows a Hall effect, but also exhibits a fully developed Hall effect with matching Hall and FET mobilities and carrier densities. This suggests that (a) even with such a low mobility, carrier delocalization in organic semiconductors is possible, and (b) Hall effect in this system may not be well described by the model based on partial carrier coherence alone. Indeed, this model predicts that systems with carrier mobilities smaller than that in pentacene should exhibit even more under-developed Hall effect with $\alpha < 1$ [29]. Therefore, our observation signals the need for further experimental and theoretical work aimed at a comprehensive understanding of charge carrier transport and Hall effect in organic semiconductors. This effort however is beyond the scope of this paper, which has its sole goal of reporting a novel, highly sensitive *ac* Hall effect measurement technique for extraction of intrinsic charge transport parameters in a wide range of low-mobility systems.

VI. CONCLUSIONS

To conclude, we have developed a powerful *ac* Hall effect measurement technique that can be used for high-precision measurements of intrinsic carrier mobility and carrier density, carried out in very low magnetic fields (smaller than 0.25 T) and capable of resolving Hall effect in OFETs with carrier mobilities as low as $0.3 \text{ cm}^2\text{V}^{-1}\text{s}^{-1}$. The method is applicable to a variety of semiconductor devices, but is particularly indispensable for investigation of the intrinsic charge transport in low-mobility systems.

ACKNOWLEDGEMENTS

We thank Michael Gershenson for helpful discussions and Hyun Ho Choi for assistance with device fabrication. We are indebted to the Institute for Advanced Materials and Devices for Nanotechnology (IAMDN) and the Department of Physics of Rutgers University for providing the necessary facilities and resources to support this project. This work has been carried out in its entirety at the Department of Physics of Rutgers University, NJ, USA. We acknowledge the financial support of this work by the National Science Foundation grant DMR-1506609.

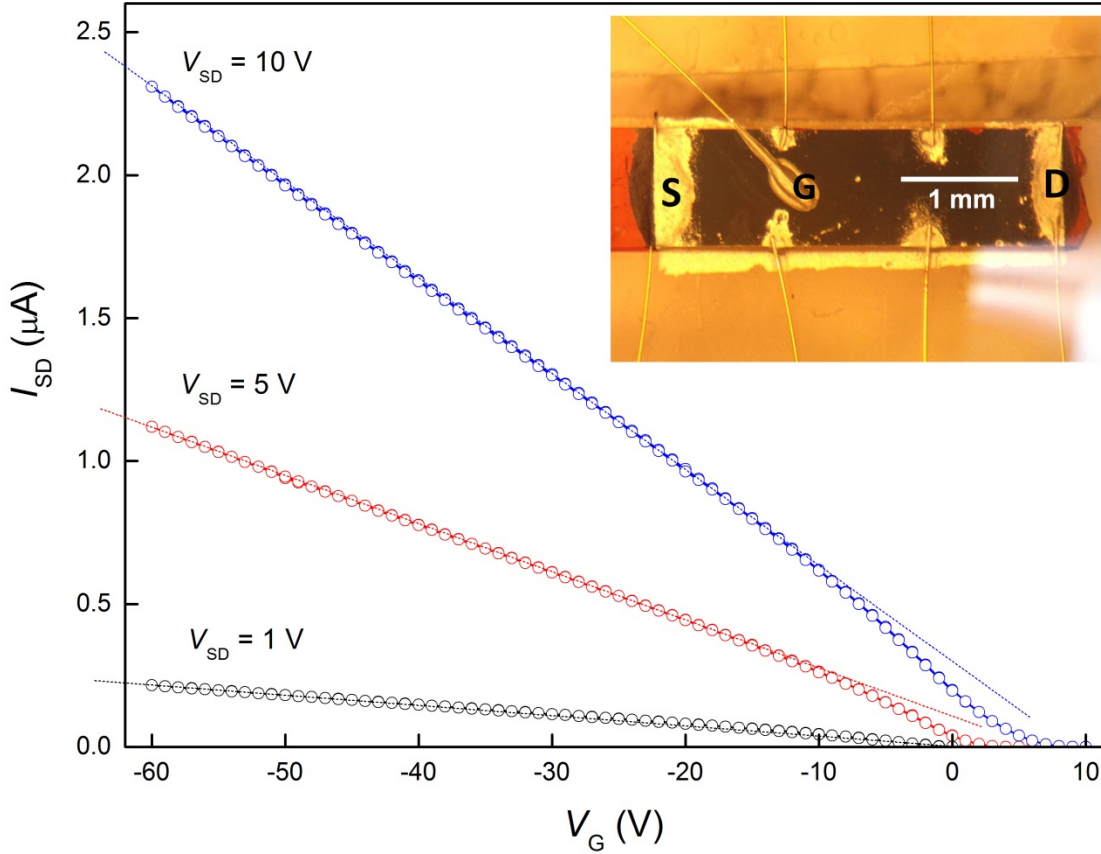


Figure 1. Transfer characteristics of a single-crystal rubrene OFET. Contacts: graphite paint, gate dielectric: parylene-*N*, gate electrode: evaporated silver. The inset shows a photo of the device. The 2-probe mobility extracted from these characteristics is independent of V_{SD} and V_G . The 4-probe mobility (not shown) is comparable to the 2-probe mobility: $\mu_{4p} \approx \mu_{2p} = 5 - 6 \text{ cm}^2\text{V}^{-1}\text{s}^{-1}$. For details on similar devices see, e.g., [7] and refs. therein.

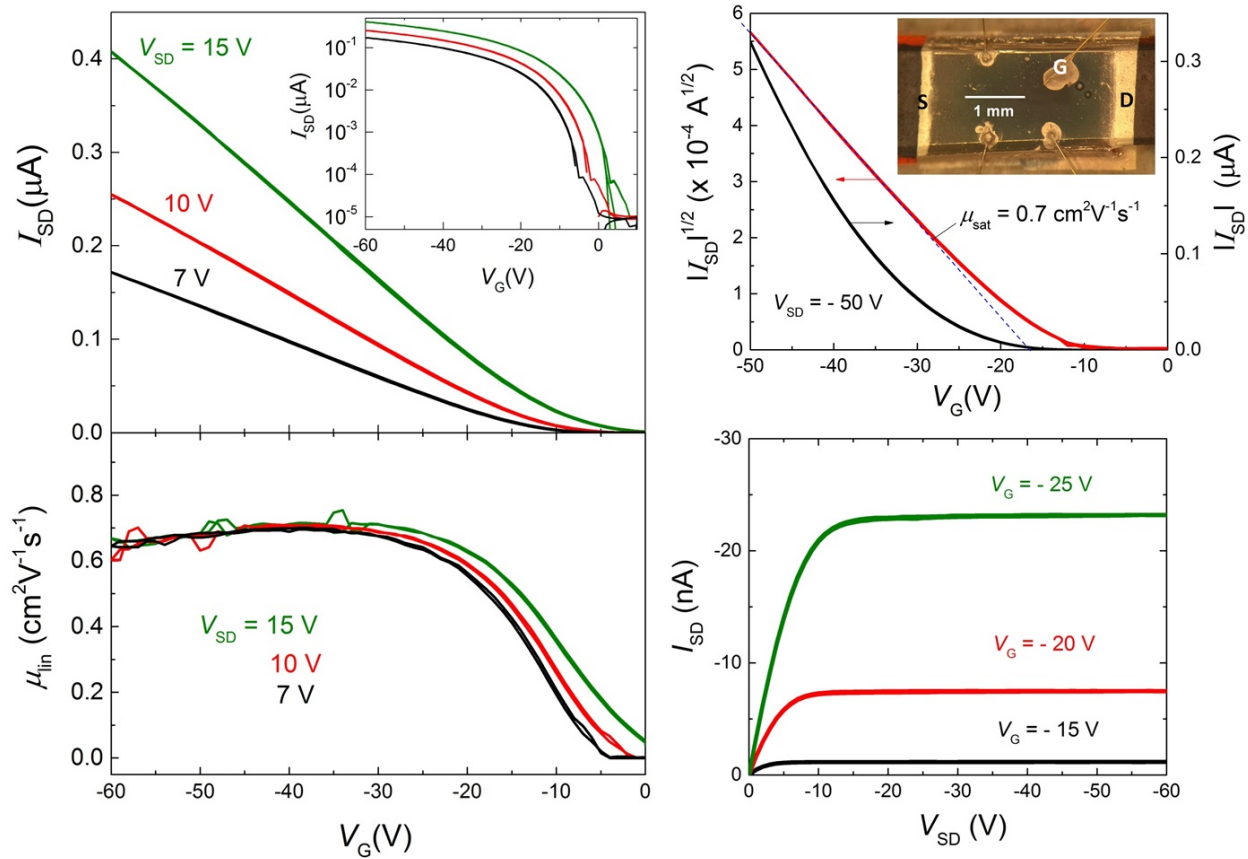


Figure 2. Characteristics of single-crystal tetracene OFETs. Contacts: graphite paint, gate dielectric: < 30 nm-thick Cytop topped with a 1.35 μm -thick parylene-*N*, gate electrode: evaporated silver. The panels show (top to bottom, left to right): linear-regime transfer curves (the inset shows the same data on a semi-log scale), linear mobility vs. gate voltage, transfer characteristics in the saturation regime (inset shows the device photo) and the output curves. These characteristics indicate that although the carrier mobility in tetracene single-crystal OFETs is relatively low (here, $\mu_{\text{lin}} \approx \mu_{\text{sat}} \sim 0.6 - 0.7 \text{ cm}^2\text{V}^{-1}\text{s}^{-1}$), the devices behave as classic text-book FETs.

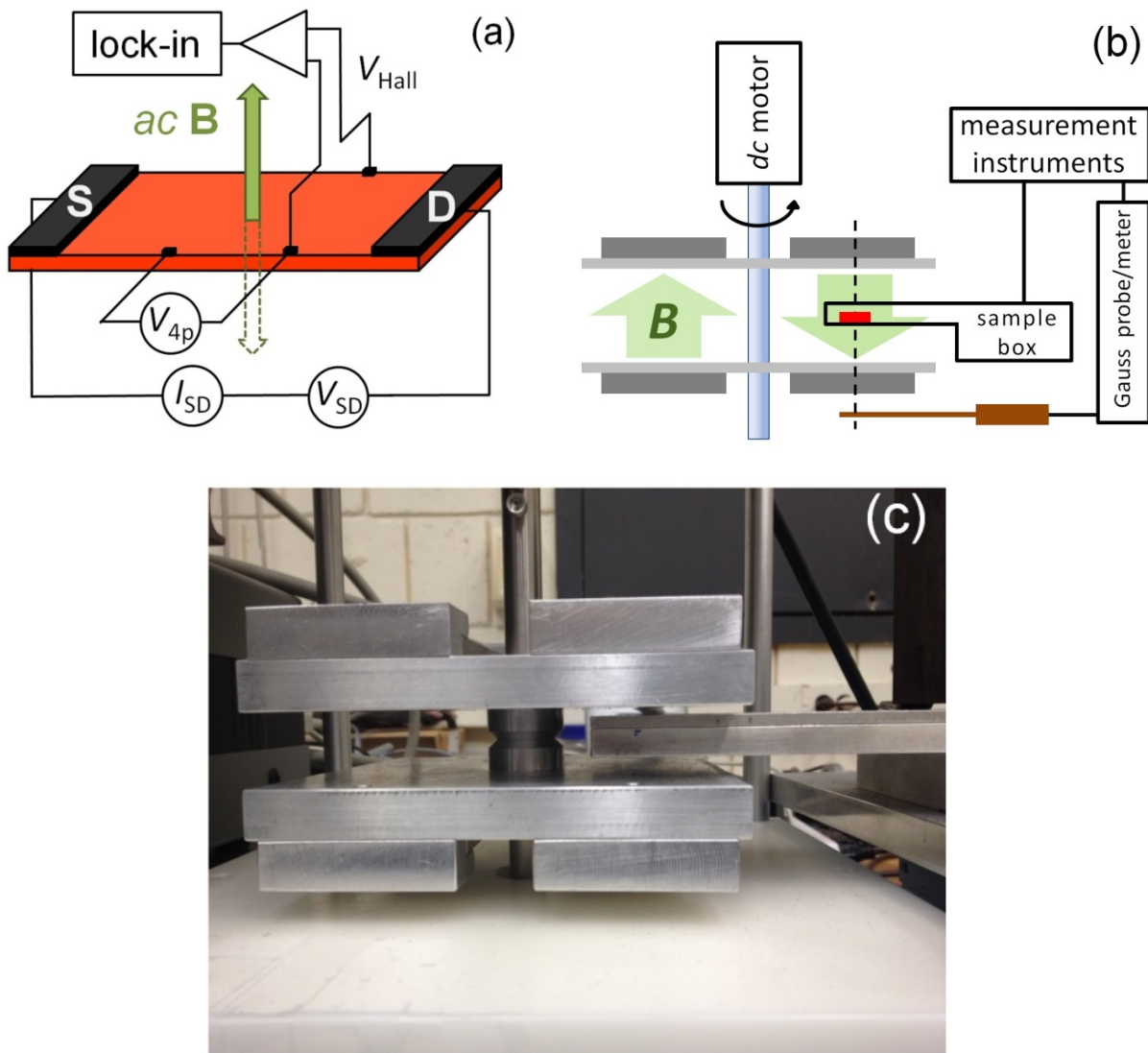


Figure 3. (a) A diagram of *ac* Hall effect measurements utilizing an *ac* magnetic field, a *dc* source-drain current excitation and a phase sensitive detection of Hall voltage (gate electrode is omitted for clarity). (b) Schematic side view of the measurement setup, showing the rotating frame with Nd magnets that create a vertical *ac* magnetic field, a sample (red) in the sample box and a Gauss meter connected to the instruments. (c) A photograph of the flat sample box inserted between the magnets. A video showing the entire setup in operation can be viewed at [24].

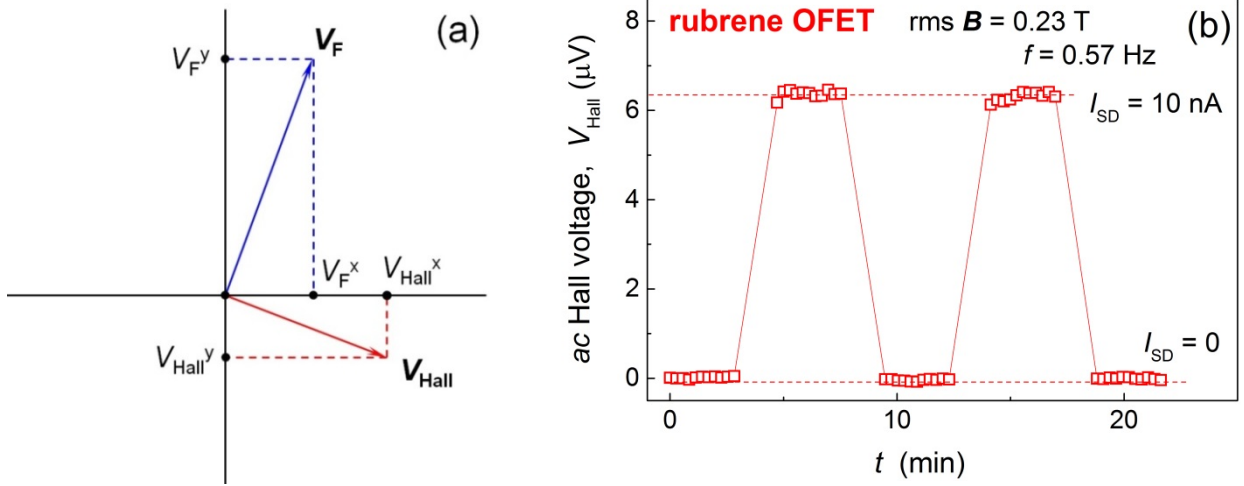


Figure 4. (a) Vector representation of the Faraday induction *emf*, V_F , and the true Hall voltage, V_{Hall} , presented across the Hall voltage leads in *ac* Hall effect measurements. The horizontal and vertical axes correspond to the signals phase shifted by 0 and $\pi/2$, respectively, relative to the reference signal supplied to the lock-in amplifier. The values measured in the experiment on the lock-in's X and Y channels are the *x* and *y* components of the total *rms* voltage detected between the Hall voltage leads, $V_{\text{H}} = V_{\text{Hall}} + V_F$. When a *dc* longitudinal current is flown through the sample ($I_{\text{SD}} \neq 0$), both V_F and V_{Hall} are generated by the *ac* magnetic field, while for zero-current excitation ($I_{\text{SD}} = 0$), only V_F is present. Thus, the true Hall voltage, $|V_{\text{Hall}}| \equiv [(V_{\text{Hall}}^x)^2 + (V_{\text{Hall}}^y)^2]^{1/2}$ can be found as $|V_{\text{Hall}}| \equiv [(V_{\text{I}}^x - V_0^x)^2 + (V_{\text{I}}^y - V_0^y)^2]^{1/2}$, where V_{I} and V_0 are the total voltages measured between the Hall leads at $I_{\text{SD}} \neq 0$ and $I_{\text{SD}} = 0$, respectively (Eq. 3). (b) *rms* value of *ac* Hall voltage measured in a single-crystal rubrene OFET in a very small *ac* magnetic field, *rms* $B = 0.23$ T ($f = 0.57$ Hz) at $V_{\text{G}} = -20$ V. The two stages of the measurement, *on* and *off*, corresponding to $I_{\text{SD}} = 0$ (set by $V_{\text{SD}} = 0$) and $I_{\text{SD}} = 10$ nA (set by $V_{\text{SD}} = 0.1$ V), are shown. Even though the Hall voltage is extremely small (~ 6 μV), the signal resolution is excellent (Hall voltage fluctuations are less than 0.3 μV). The Hall mobility and carrier density extracted from these data, $\mu_{\text{Hall}} = 5.8 \pm 0.05$ $\text{cm}^2\text{V}^{-1}\text{s}^{-1}$ and $n_{\text{Hall}} = (2.26 \pm 0.02) \times 10^{11}$ cm^{-2} , agree well with those obtained in 4-probe longitudinal FET measurements.

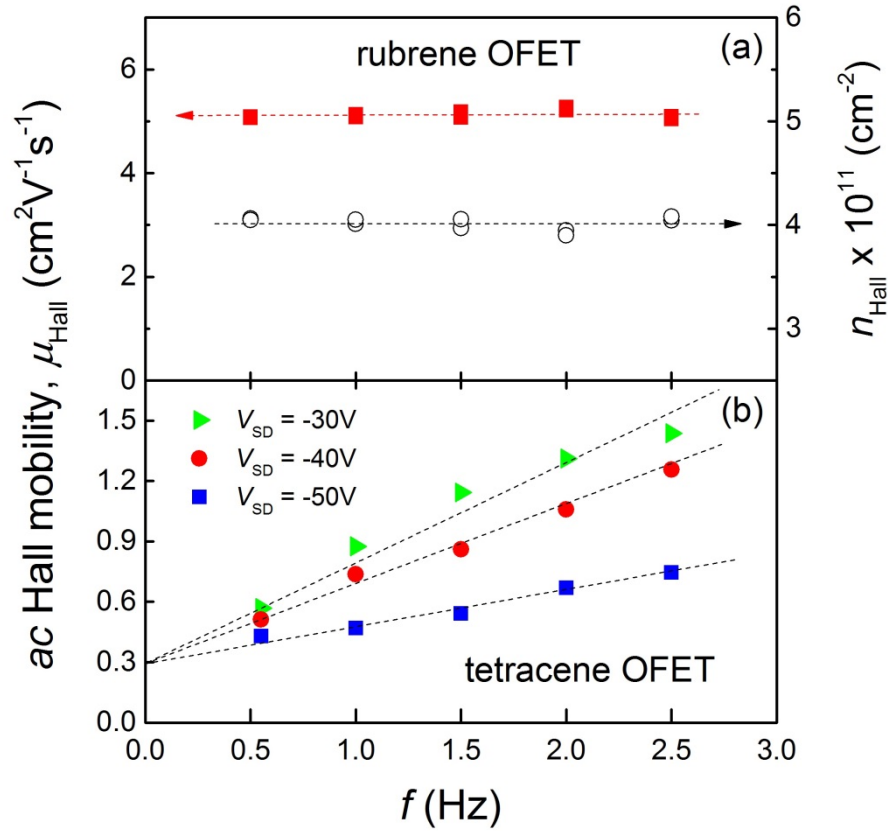


Figure 5. Dependence of the apparent *ac* Hall mobility on the frequency of *ac* *B* field in two representative systems, with the intrinsic Hall mobility μ_0 identified as the zero-frequency offset: (a) single-crystal rubrene OFETs, where μ_{Hall} and n_{Hall} , measured at *rms* $B = 0.23$ T, $V_G = -30$ V and $I_{\text{SD}} = 100$ nA (set by $V_{\text{SD}} = 1$ V), are found to be frequency independent, yielding the intrinsic Hall mobility $\mu_0 = 5.1$ $\text{cm}^2\text{V}^{-1}\text{s}^{-1}$; (b) single-crystal tetracene OFETs, where the linear fits to the frequency dependence obtained at three different V_{SD} converge at the same zero-frequency limit, yielding the intrinsic Hall mobility $\mu_0 = 0.3$ $\text{cm}^2\text{V}^{-1}\text{s}^{-1}$.

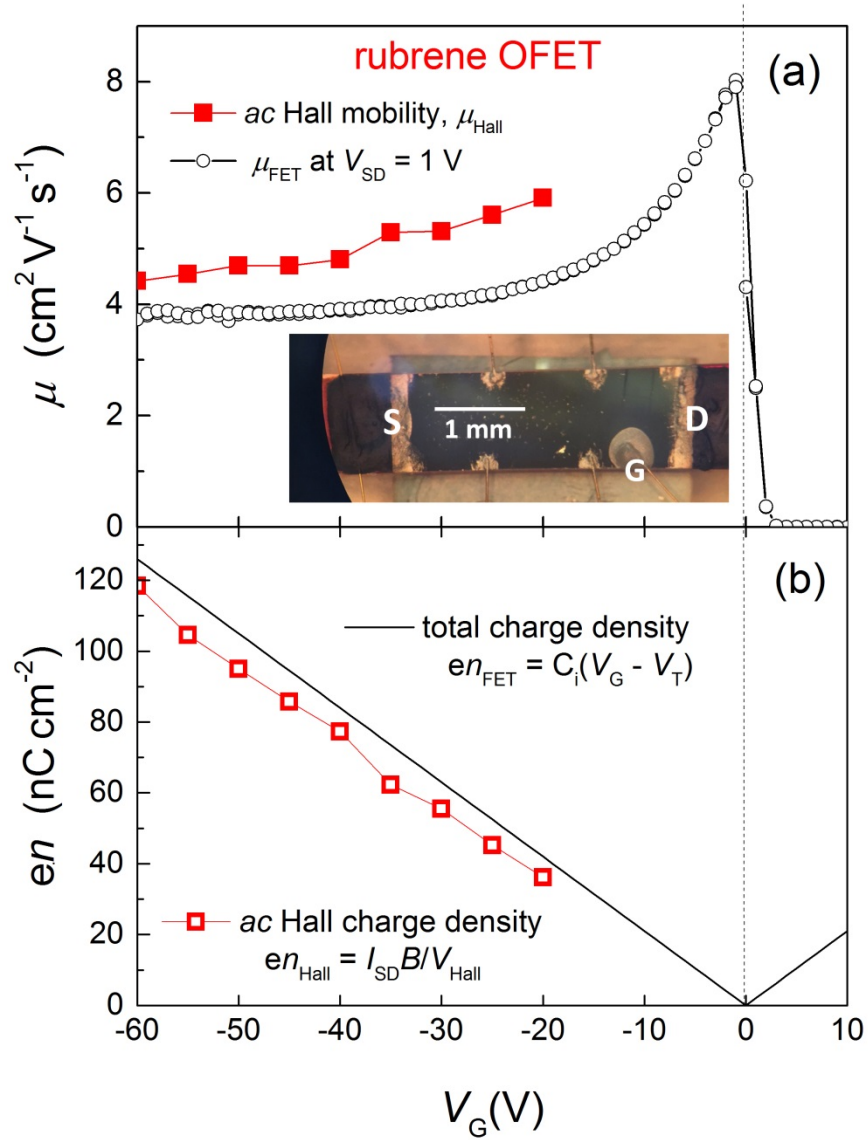


Figure 6. ac Hall effect ($B_{\text{rms}} = 0.23 \text{ T}$) and conventional FET measurements in single-crystal rubrene OFETs. (a) A linear-regime FET mobility (open circles) is compared with the mobility obtained in ac Hall measurements (solid squares). (b) The total electrostatic carrier density (solid line) is compared with the carrier density extracted from ac Hall measurements using Eq. 4 (open squares). A good match between Hall effect and FET carrier mobilities and densities is observed, as expected for a coherent transport of delocalized carriers and consistent with the prior observations in dc Hall effect studies of rubrene OFETs.

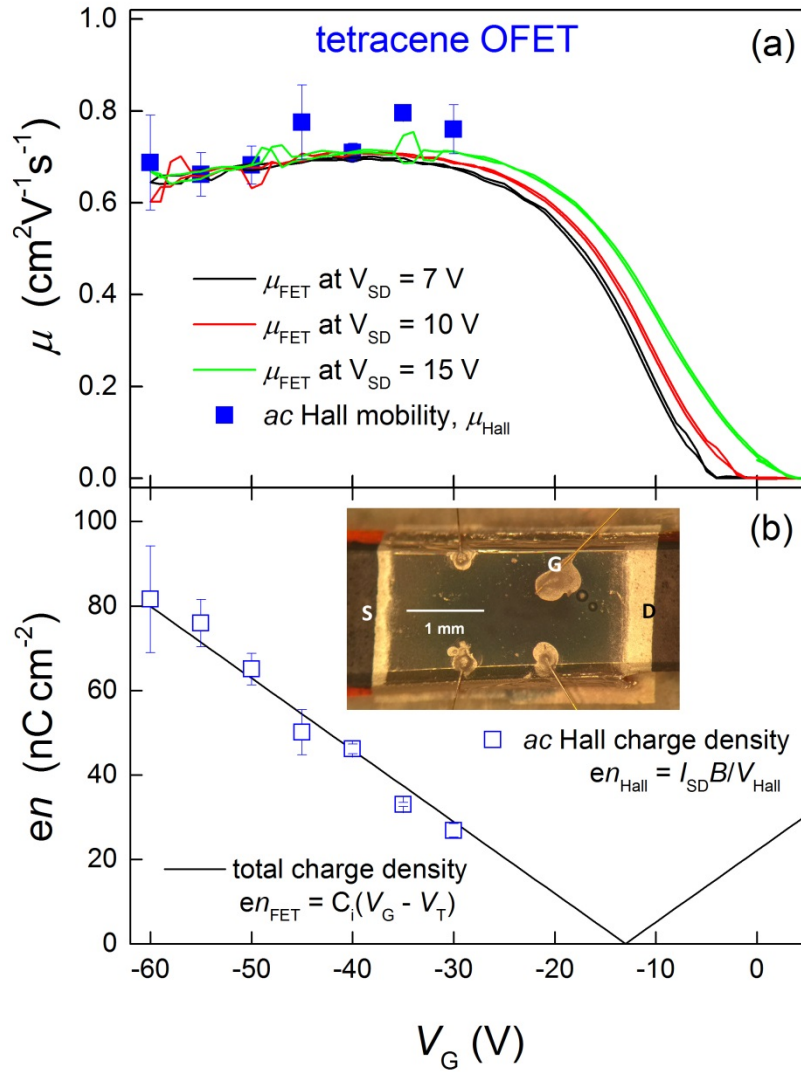


Figure 7. *ac* Hall effect ($B_{\text{rms}} = 0.23$ T) and conventional FET measurements in single-crystal tetracene OFETs. (a) A linear-regime FET mobility measured at three different V_{SD} values (solid lines) is compared with the mobility extracted from *ac* Hall measurements (solid squares). (b) The total electrostatic carrier density (solid line) and the carrier density extracted from *ac* Hall measurements using Eq. 4 (open squares) as a function of V_G . Contrary to the common expectation, this low- μ system exhibits a Hall effect with a good match between the Hall and FET carrier densities and mobilities, indicating that even when mobility is below $1 \text{ cm}^2\text{V}^{-1}\text{s}^{-1}$, charge carriers in organic semiconductors can be coherent.

REFERENCES

- [1] D. A. da Silva Filho, E.-G. Kim, and J.-L. Bredas, Transport Properties in the Rubrene Crystal: Electronic Coupling and Vibrational Reorganization Energy, *Adv. Mater.* **17**, 1072 (2005).
- [2] J. L. Bredas, D. Beljonne, V. Coropceanu, and J. Cornil, Charge-transfer and energy-transfer processes in pi-conjugated oligomers and polymers: a molecular picture, *Chem. Rev.* **104**, 4971 (2004).
- [3] V. Coropceanu, J. Cornil, D. A. da Silva, Y. Olivier, R. Silbey, and J. L. Bredas, Charge transport in organic semiconductors, *Chem. Rev.* **107**, 926 (2007).
- [4] K. Hannewald and P. A. Bobbert, *Ab initio* theory of charge-carrier conduction in ultrapure organic crystals, *Appl. Phys. Lett.* **85**, 1535 (2004).
- [5] A. Troisi and G. Orlandi, Charge-Transport Regime of Crystalline Organic Semiconductors: Diffusion Limited by Thermal Off-Diagonal Electronic Disorder, *Phys. Rev. Lett.* **96**, 086601 (2006).
- [6] D. L. Cheung and A. Troisi, Modelling charge transport in organic semiconductors: from quantum dynamics to soft matter, *Phys. Chem. Chem. Phys.* **10**, 5941 (2008).
- [7] V. Podzorov, Organic single crystals: Addressing the fundamentals of organic electronics, *MRS Bulletin* **38**, 15-24 (2013).
- [8] S. M. Sze, *Physics of Semiconductor Devices*, Wiley, New York (1981).
- [9] S. Ciuchi and S. Fratini, Electronic transport and quantum localization effects in organic semiconductors, *Phys. Rev. B* **86**, 245201 (2012).
- [10] R.S. Sánchez-Carrera, P. Paramonov, G. M. Day, V. Coropceanu, and J.-L. Brédas, Interaction of Charge Carriers with Lattice Vibrations in Oligoacene Crystals from Naphthalene to Pentacene, *J. Am. Chem. Soc.* **132**, 14437 (2010).
- [11] C. Krellner, S. Haas, C. Goldmann, K. P. Pernstich, D. J. Gundlach, and B. Batlogg, Density of bulk trap states in organic semiconductor crystals: Discrete levels induced by oxygen in rubrene, *Phys. Rev. B* **75**, 245115 (2007).
- [12] R. Noriega *et al.*, A general relationship between disorder, aggregation and charge transport in conjugated polymers, *Nature Mater.* 10.1038/nmat3722 (2013).
- [13] V. Podzorov, E. Menard, J. A. Rogers, and M. E. Gershenson, Hall Effect in the Accumulation Layers on the Surface of Organic Semiconductors, *Phys. Rev. Lett.* **95**, 226601 (2005).
- [14] J. Takeya, K. Tsukagoshi, Y. Aoyagi, T. Takenobu, and Y. Iwasa, Hall Effect of Quasi-Hole Gas in Organic Single-Crystal Transistors, *Jpn. J. Appl. Phys.* **44**, L1393 (2005).
- [15] S. Wang, M. Ha, M. Manno, C. D. Frisbie, and C. Leighton, Hopping transport and the Hall effect near the insulator–metal transition in electrochemically gated poly(3-hexylthiophene) transistors, *Nature Commun.* 3:1210 doi:10.1038/ncomms2213 (2012).
- [16] W. Xie, S. Wang, X. Zhang, C. Leighton, and C. D. Frisbie, High Conductance 2D Transport around the Hall Mobility Peak in Electrolyte-Gated Rubrene Crystals, *Phys. Rev. Lett.* **113**, 246602 (2014).
- [17] N. A. Minder, S. Ono, Z. Chen, A. Facchetti, and A. F. Morpurgo, Band-Like Electron Transport in Organic Transistors and Implication of the Molecular Structure for Performance Optimization, *Adv. Mater.* **24**, 503 (2012).
- [18] T. Holstein, Hall Effect in Impurity Conduction, *Phys. Rev.* **124**, 1329 (1961).

-
- [19] R. S. Klein, Investigation of the Hall effect in impurity-hopping conduction, *Phys. Rev. B* **31**, 2014 (1985).
- [20] R. W. I. de Boer, M. E. Gershenson, A. F. Morpurgo, V. Podzorov, Organic single-crystal field-effect transistors, *Phys. Stat. Solidi* **201**, 1302 (2004).
- [21] V. Podzorov, V. M. Pudalov, M. E. Gershenson, Field-effect transistors on rubrene single crystals with parylene gate insulator, *Appl. Phys. Lett.* **82**, 1739 (2003).
- [22] V. Podzorov, S. E. Sysoev, E. Loginova, V. M. Pudalov, M. E. Gershenson, Single-crystal organic field effect transistors with the hole mobility ~ 8 cm²/Vs, *Appl. Phys. Lett.* **83**, 3504 (2003).
- [23] Y. Xia, V. Kalihari, C. D. Frisbie, N. K. Oh, J. A. Rogers, Tetracene air-gap single-crystal field-effect transistors, *Appl. Phys. Lett.* **90**, 162106 (2007).
- [24] A video of the *ac* Hall effect measurement setup in operation can be viewed here:
<http://www.physics.rutgers.edu/~podzorov/>
- [25] B. Blülle, R. Häusermann, and B. Batlogg, Approaching the Trap-Free Limit in Organic Single-Crystal Field-Effect Transistors, *Phys. Rev. Appl.* **1**, 034006 (2014).
- [26] C. R. Newman, R. J. Chesterfield, J. A. Merlo, and C. D. Frisbie, Transport Properties of Single-Crystal Tetracene Field-Effect Transistors with Silicon Dioxide Gate Dielectric, *Appl. Phys. Lett.* **85**, 422 (2004).
- [27] T. Uemura, M. Yamagishi, J. Soeda, Y. Takatsuki, Y. Okada, Y. Nakazawa, and J. Takeya, Temperature dependence of the Hall effect in pentacene field-effect transistors: Possibility of charge decoherence induced by molecular fluctuations, *Phys. Rev. B* **85**, 035313 (2012).
- [28] J. Takeya, *Chemical Science of π -Electron Systems*, pp. 589-604, Springer (2015).
- [29] T. Fukami, H. Ishii, N. Kobayashi, T. Uemura, K. Sakai, Y. Okada, J. Takeya, and K. Hirose, Correlation between thermal fluctuation effects and phase coherence factor in carrier transport of single-crystal organic semiconductors, *Appl. Phys. Lett.* **106**, 143302 (2015).